ROMANIAN JOURNAL OF INFORMATION SCIENCE AND TECHNOLOGY
Volume **11**, Number 1, 2008, 71–84

Controlled X-Ray Induced Gold Nanoparticles Deposition

R. DIVAN[1], Q. MA[2], D. C. MANCINI[1], D. T. KEANE[2]

[1] Center for Nanoscale Materials, Argonne National Laboratory,
9700 South Cass Avenue, Argonne, IL 60439, USA

E-mail: divan@aps.anl.gov

[2] DND-CAT, Northwestern University Synchrotron Research Center,
9700 South Cass Avenue, Argonne, IL, 60439, USA

Abstract. This paper outlines new approaches for utilizing X-rays for gold nanoparticles deposition by performing Surface Photochemistry Induced by X-ray Irradiation (SPIXI). High-energy synchrotron radiation was used to induce the deposition of gold nanoparticles from a gold-salt solution onto different surfaces. By controlling the deposition parameters (dose, solution, surfactants, and stabilizer polymer concentrations), the distribution and average size of the nanoparticles can be influenced. The distribution of the deposited particle heights and diameters at low doses suggests there is a mechanism of growth of the particles after nucleation on the surface.

1. Introduction

Due to their unique electrical and optical properties, preparation of metal nanoparticles on various substrates is a key issue in all fields of modern science and technology covering electronics (single electron transistors), photonics, catalysis, biochemical sensors. Nowadays nanotechnology promises great improvement of human life by providing more efficient catalysts, and new effective drugs.

Nanoparticles-based electrodes on boron-doped diamond perform as excellent catalysts for oxygen reduction [1]. The discovery of distinctive catalytic properties of dispersed gold nanoparticles on oxide supports has stimulated extensive research activities: the size of the gold particles substantially affects the catalytic activity, and the gold nanoparticles must be smaller than 5 nm for high catalytic activity to occur [2].

Nanoparticles have been found to be useful in the development of systemic, oral, pulmonary, transdermal and other administration routes to study drug targeting, the enhancement of drug bioavailability and protection of drug bioactivity and stability [3–6]. They are able to penetrate the cells to facilitate cellular internalization and connective tissue permeation, thus enabling the drugs to be delivered efficiently to the targeted tissue without clogging the capillaries.

In addition to the conventional gas phase, electrochemical or electroless wet chemical deposition methods, techniques utilizing lasers, ion-beams, electron-beam, and the high-energy X-rays produced by synchrotron radiation sources were reported to produce nanocrystalline metallic deposition onto different substrates in the desired chemical and morphological state(s) [7–9]. Use of energetic beams and X-rays is particularly attractive since lithographic techniques can also be introduced for patterning/direct-writing purposes, directly producing metallic patterns in the form of macroscopically-continuous, but nanoscopically fragmented films, in a single lithographic step [9, 10].

The high-energy X-rays produced by the Advanced Photon Source (APS) at Argonne National Laboratory (ANL) have deep penetration lengths for low-Z materials. Therefore, they can be used to induce chemical reactions on surfaces of solids immersed in liquids containing low-Z molecules [7, 8]. If the liquid contains a metal salt, the X-ray irradiation induces deposition of metallic films that can be in either polycrystalline or nanocrystalline forms. The X-ray-induced gold deposition on a SiO_2/Si surface is a gold-ion reduction process in which it is likely that X-ray-generated photoelectrons reduce the ions to neutral metal[8]. During the irradiation, Au nanoparticles precipitate from the solution. The process is indicated by the color change of the solution, from colorless to dark amber, consistent with the size of the nanoparticles also observed in the deposit on the substrate (20–50 nm)[11].

The purpose of this paper is to present our results on gold nanoparticle deposition induced by X-rays. We investigate the early steps of the deposition process, prior to obtaining continuous films, when the deposited pattern is formed by clusters of metallic nanoparticles. The process variables include: substrate type, reactant, surfactant concentration, polymer stabilizer, pH, exposure time, beam current, X-ray cutoff energy or X-ray energy (monochromatized beamline). By controlling the deposition parameters, the distribution and average size of the nanoparticles can be influenced. The particle sizes in these depositions range from a few nanometers at the smaller end to ∼30 nanometers at the larger end.

Special attention is focused on the differences between GaAs and SiO_2 and on the influence of surfactants and stabilizer polymers on nanoparticle size.

2. Experimental

X-ray induced deposition experiments were carried out at the bending magnet beamline (5-BM-D), operated by DND-CAT, at the Advanced Photon Source. The beamline extracts 2-mrad dipole radiation beam, which can be configured to deliver either white or “pink” beams into the experimental station. The experimental station is about 60 meters from the radiation source. In this work, the pink beam is selected

using a pair of Rh-coated mirrors set at the incidence angle of 0.17 degrees, which delivers the X-ray photons with energies ranging from ∼4 keV to ∼20 keV as analyzed by a solid state detector. The second Rh-coated mirror is bent to focus the pink beam vertically to a size of about 250 microns at FWHM. A Huber slit and a beam shutter (X-ray instrument associate) are used to select the horizontal beam size and to execute exposure control. For all the X-ray exposures, the X-ray beam size is set at 0.25×4 mm^2. The synchrotron storage ring was operated in the "top-up" mode with the electron beam current kept around 100-mA. The dose measurements using a TLD 700 detector indicated that a five-minute exposure has rendered a dose of 300 krad or a rate of 60 krad/min.

A radiation-resistant plastic cell is used to house the solution, the samples, and the X-ray mask [9]. The cell also has an inlet and an outlet, which are connected to a closed-loop pumping system that has a filter at the outlet and a fresh solution reservoir connected to the inlet. The solution in the cell is freshened during the X-ray exposure. The X-ray mask was fabricated at APS and is composed of a 70-μm-thick gold pattern on a 250-μm-thick graphite sheet [12]. The metal-containing solutions used for deposition were a sodium gold sulfite $[Au(SO_3)_2]Na_3$ electroplating solution (10g/l Au, Neutronex 309, Enthone-OMI Inc) with a pH of 9.5, and a 0.5 mM aqueous solution of tetrachloroauric acid ($HAuCl_4$:$4H_2O$) (Aldrich) with pH value of 2.8 as measured by a pH meter (ORION-290A). Surfactants (nonionic: Triton X-100, anionic: SDS sodium dodecyl sulfate), and a polymer capping agent (alkyl thioether end-functionalized poly(methacrylic acid)) have been used [13]. All surfactant solutions were prepared in DI water. The critical micelle concentration (cmc) in the deposition solution was calculated with the formula:

$$\lg(\text{cmc}) = -3{,}7671-0{,}2133\lg(\text{cm} + [\text{OH}] + [\text{KBr}]),$$

where cm is the critical micelle concentration of the surfactant in pure water [14].

The samples were cut from n-type Si (100) wafers covered with 1-μm-thick thermal oxide. The GaAs (100) wafers were n- and p-type (ATRAMET, Inc.). The n-type GaAs is doped with Si at 10^{17} to 2×10^{18} cm^{-3}, and the p-type GaAs is doped with Zn at $1–5\times10^{17}$ cm^{-3}. The wafers were cut into various sizes of rectangular pieces. In a separate experiment, we used pre-patterned GaAs samples by optical lithography with MA6 (Karl Suss) and by e-beam lithography with Raith 150 (Karl Suss).

Particle characterization was performed by atomic force microscopy (AFM) using a TopoMetrix Explorer AFM with a Si cantilever tip, a Tencor Alphastep 500 profilometer, and scanning electron microscopy (SEM) with Raith 150.

3. Results and discussion

Figure 1 illustrates the radiation source in two different aspects: a) the 2-mrad, pink X-ray flux delivered from the 5-BMD bending magnet beamline and b) the absorbed X-ray doses measured using radiochromic films (HD-810) at the sample position.

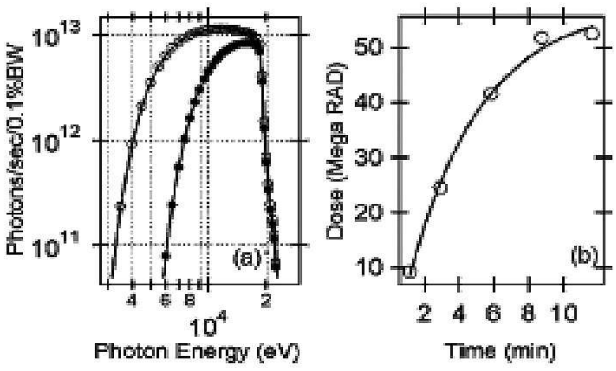

a) b)

Fig. 1. (a) Pink X-ray spectrum delivered from the 5-BMD bending magnetic beamline (open circles) and the spectrum of the photons impinging on the sample surface (solid circles); (b) The X-ray doses measured using radiochromic films (HD-810).

The open circles in Fig. 1a are obtained for X-ray beam after all the beamline optics, and the solid circles in Fig. 1a are obtained after the absorption by 2-mm solution is taken into account. At the sample position, the X-ray flux is $\sim 2\times10^{16}$ photons/sec for a 0.25×4-mm^{2}beam. The number of equivalent *band gap* photons may be estimated as 2×10^{16}times the X-ray energy divided by the band gap ($E_g \sim$ 1.43 eV), which gives $\sim10^{19}$ photons/sec. The use of HD-810 films in this energy range (4 to 20 keV) does not warrant precise measurements of the doses since the sensitivity is energy dependent. Under the experimental conditions, the thermal effect is not a concern due to the selected small portion of emitted X-rays and the large volume of solution [15].

3.1. Deposition on SiO_2 surface

The following experiments were designed and executed: (a) dose dependence, (b) energy dependence, (c) dilution dependence, (d) particle size controlled by surfactants, (e) particle size controlled by stabilizer polymer, and (f) solution-type dependence.

The deposited metallic film using Neutronex solution shows individual particles between 7 and 70 nm in diameter for lower exposure doses, and the appearance of the agglomerates of spherical particles at higher exposure doses (Fig. 2).

From AFM measurements the height of the nanoparticles remains nearly constant while the dose is increased. The deposition of new small gold nanoparticles occurs preferentially between the existing deposited Au nanoparticles. Liz-Márzan has reported similar results, large nanoparticles seemed to be formed during the first steps of the deposition, increasing the proportion of smaller nanoparticles [16].

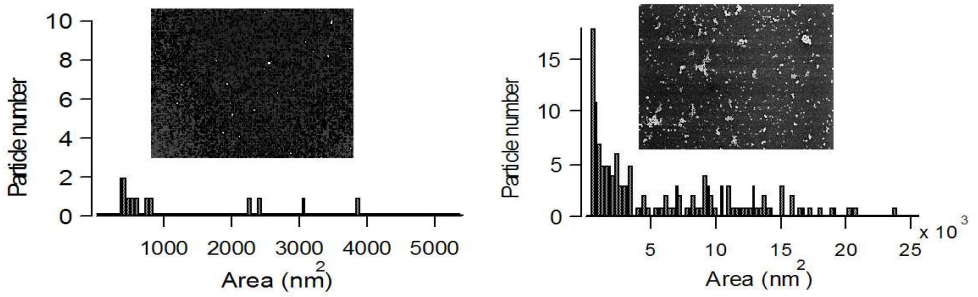

a) b)

Fig. 2. SEM micrographs (15 000×) and size distribution of gold nanoparticles deposited on SiO_2: (a) dose of 0.5 Mrad); (b) dose of 40 Mrad.

The distribution of the nanoparticles is more uniform for 50% aqueous solution of Neutronex (Fig. 3).

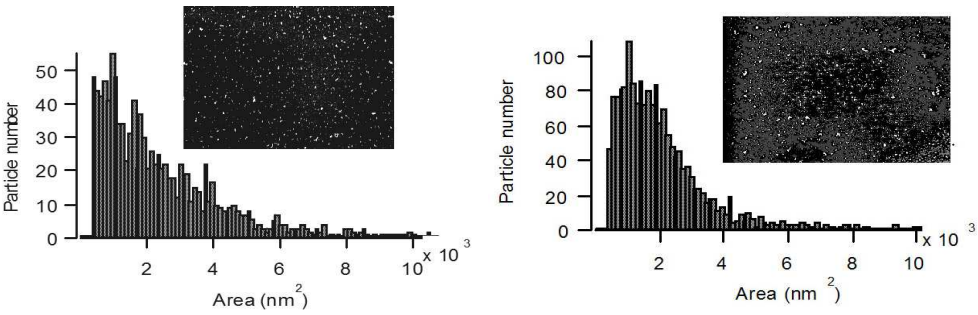

a) b)

Fig. 3. SEM micrographs (15 000×) and size distribution of gold nanoparticles deposited on SiO_2, dose 144 Mrad, for different dilutions: (a) 100%; (b) 50% Neutronex.

Figure 4 compares two results obtained with and without attenuation of the incoming X-ray beam. It can be seen that attenuating the beam does have an effect on the particle distribution.

The use of a 500 μm Al filter cuts X-ray photons with energies lower than 9 keV dramatically. These results apparently show that the particle distribution depends on the X-ray photon energy. However, the total photon flux is lower as well. To differentiate between these two factors, *i.e.*, photon energy *vs.* photon flux, more elaborated experiments that allow quantitative analysis have to be carried out.

We have noticed nanoparticle clusters formation on SiO_2 substrates already at very low doses. Experience in direct chemical synthesis of metal colloids shows that mono-disperse nanoparticles can be obtained when arresting their growth by using a capping agent, while prevention of clustering can be achieved by using surfactants [13, 16, 17].

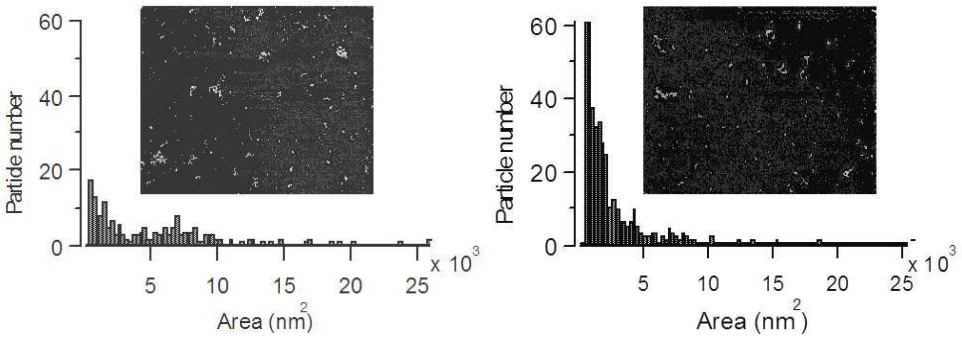

a) b)

Fig. 4. SEM micrographs (15 000×) and size distribution of gold nanoparticles deposited on SiO_2, dose 40 Mrad, (a) no filter, (b) with 500 μm Al filter.

Addition of SDS to 50% Neutronex solution has not suppressed nanoparticle clusters appearance (Fig. 5). The deposition has been observed only when we increased the dose at 144 Mrad. For high concentration of SDS (8 mM) we have noticed nanoclusters formation (Fig. 5a) and at lower concentration (4 mM) small particles with an average diameter of 20 nm were formed (Fig. 5b).

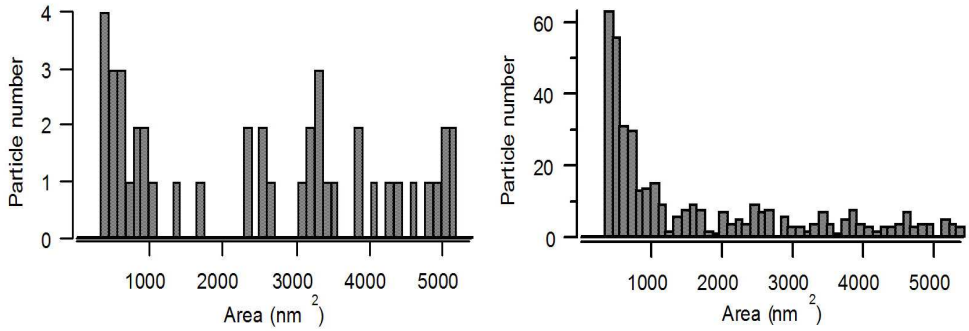

a) b)

Fig. 5. Size distribution of deposited gold nanoparticles from 50% Neutronex with SDS: (a) 8 mM, (b) 4 mM.

Recently research noticed that spherical gold nanoparticles are obtained for weakly bound counterions such as SO_4^{2-}[18]. The surfactant molecules are adsorbed from the aqueous solution onto gold surface at low surfactant concentrations and smaller particles were formed. High concentration of surfactant favoured the formation of gold nanoclusters.

Similar results have been obtained for non-ionic surfactant Triton X-100.

Addition of 0.03 mM and 0.05 mM of alkyl thioether end-functionalized poly(methacrylic acid) at 50% Neutronex solution improved the dispersion of deposited nanoparticles on the surface but still nanoclusters have formed (Fig. 6).

Based on the fact that we have not obtained mono-disperse nanoparticles in the range of 2–5 nm by adding surfactants and stabilizer polymers to the commercial solution, we have considered that the unknown composition of the solution may be the cause.

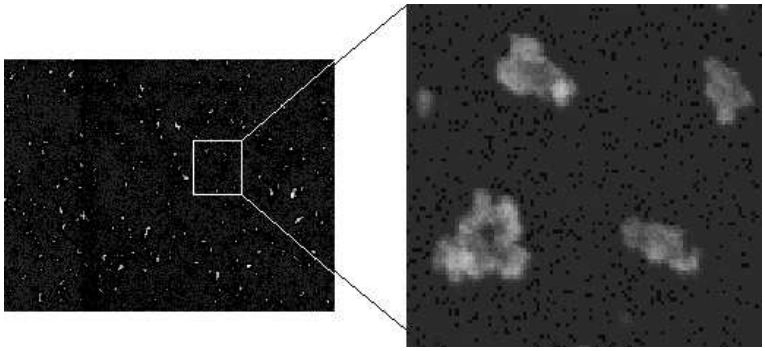

Fig. 6. SEM micrographs of deposited gold nanoparticles from 50% Neutronex with 0.5 mM polymer.

Similar experiments have been conducted using an aqueous solution of 0.5 mM hydrogen tetrachloroaurate without (Fig. 7a), and with 0.03 mM stabilizer polymer (Fig. 7b).

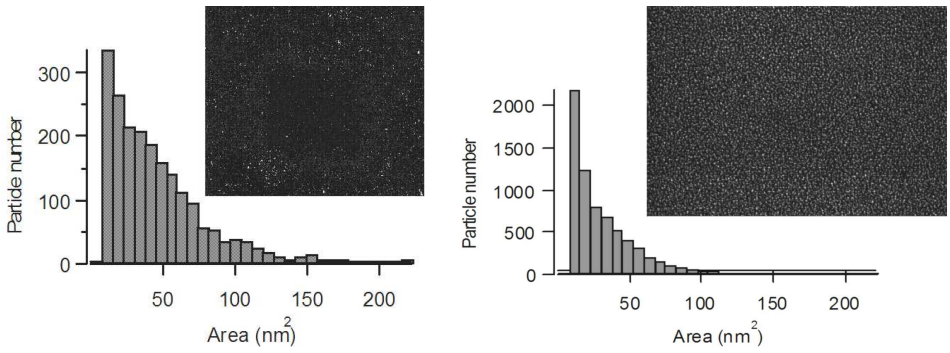

a) b)

Fig. 7. SEM micrographs (60 000×) and size distribution of gold nanoparticles deposited on SiO_2, dose 144 Mrad, 0.5 mM hydrogen tetrachloroaurate: (a) without polymer, (b) with 0.03 mM polymer.

The images (Figs. 6 and 7) confirm the effect of the solution and show a very narrow size distribution in the sub-5 nm size range when the capping polymer is added to the hydrogen tetrachloroaurate solution.

The beam energy and the solution conditions permit the control of the Au nanoparticles deposition (Fig. 4 and Fig. 7). The distribution is more uniform at higher energy and higher dilution. The stabilizer polymer prevents the nanocluster formation.

The defects on the silicon dioxide surface can dominate the nucleation behaviour too. Small crystal nuclei form but unless their size exceeds a critical value (critical

nucleus), they will re-dissolve rather than grow [19]. The distribution of the deposited particle heights and diameters in the early stages of deposition (low doses) suggests there is a mechanism of growth of the particles after nucleation on the silicon dioxide surface.

Patterned gold deposition can be obtained by using an X-ray mask. The deposition occurs on the beam-illuminated area. Figure 10 shows the SEM image of a patterned 40-nm-thick Au deposit on silicon dioxide using 50% Neutronex solution at 423 Mrad. The film consists of discrete, uniformly sized grains of average lateral size of about 100 nm, as indicated by AFM and SEM measurements. The resolution is limited by the aspect ratio of the X-ray mask.

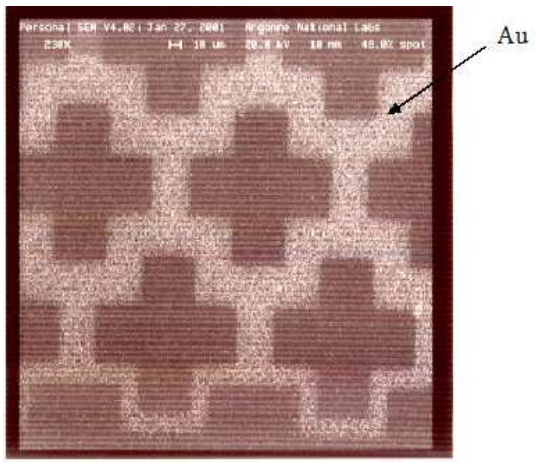

Fig. 8. SEM image of a patterned Au-deposited nanostructured layer on silicon dioxide [9].

3.2. Deposition on GaAs surface

It is established that the surface states will cause the band bending of a doped semiconductor at the surface. For n-type GaAs, the band will bend upwards and the positive charges (holes) will accumulate at the surface, forming a space-charging region between the surface and the bulk. In other words, the n-type GaAs surface is *anodic*. For p-type GaAs, the band will bend downwards and the negative charges (electrons) will accumulate at the surface. Therefore, the p-type surface is *cathodic*. Given the band structure at the surface, the dark etching already occurs for an n-type GaAs surface in an acid solution through [20–22]:

$$\mathrm{GaAs} + 6\mathrm{h}^{+}_{\mathrm{VB}} \rightarrow \mathrm{Ga}^{3+} + \mathrm{As}^{3+}$$

Conversely, the metal deposition may occur on a p-type GaAs surface through:

$$\mathrm{Metal}^{+} + e^{-}/\mathrm{p\text{-}GaAs} \rightarrow \mathrm{Metal/p\text{-}GaAs}$$

The exposure experiments with n- and p-type GaAs samples and 50% Neutronex solution are similar to the findings reported by Hoisty using the laser light [23]. The deposition occurred on the beam-illuminated area for the p-type samples while on the non-illuminated area for the n-type samples. In the latter case, noticeable etching occurs in the beam-illuminated area. The deposits have distinctly different morphology. On the p-type sample, rapid growth of single particles is observed. The particle size exceeds 150 nm for a 5-min exposure (Fig. 11).

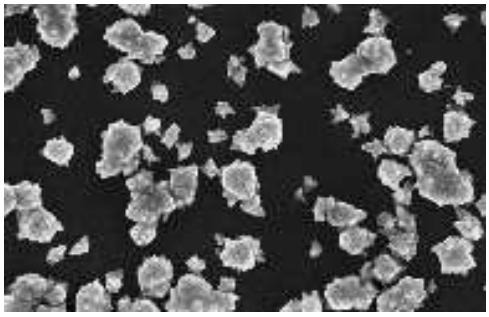

Fig. 9. SEM image (35 000×) of gold nanoparticles deposited on p-GaAs by SPIXI from 50% Neutronex solution.

The particle shape is more irregular with flake-like morphology and the final deposition appears to be courser.

On the n-type sample, the deposition starts out with formation of small particles of sub-nanometer sizes, which do not grow in size but coalesce with adjacent ones over the time of exposure. For a 5-min exposure, the particle size is estimated to be about 20 nm in diameter. The final products are smooth films with shinning gold appearance.

Figure 10 shows the particle distributions for a series of depositions (upper panel) as a function of exposure time (or dose) and two scanning electron micrographs (SEM) (lower panel), for n-type samples. The number of small particles increases with time initially, and decreases for longer exposure. This change is caused by the onset of particle coalescence, as can be seen in the SEM images (the left is for 1.5-min exposure and the right is for 6-min exposure).

To make a micro- or nano-structure through this deposition process, the lithography patterning technique is used for an n-type GaAs substrate, since selective deposition will be achieved by masking certain areas to prevent direct contact to the solution. Figure 11 illustrates the steps used to achieve the patterned deposition.

The sample surfaces are spin coated with a layer of photoresists (Shipley S1805) or PMMA, and are subsequently patterned either using optical lithography through an optical mask with dual polarity structures or low-energy e-beam writer.

After spin coating, patterning and developing, the sample is placed in the liquid cell and undergoes stationary X-ray exposure under the conditions described above. Following the X-ray exposure the photoresist is removed to reveal the deposited features.

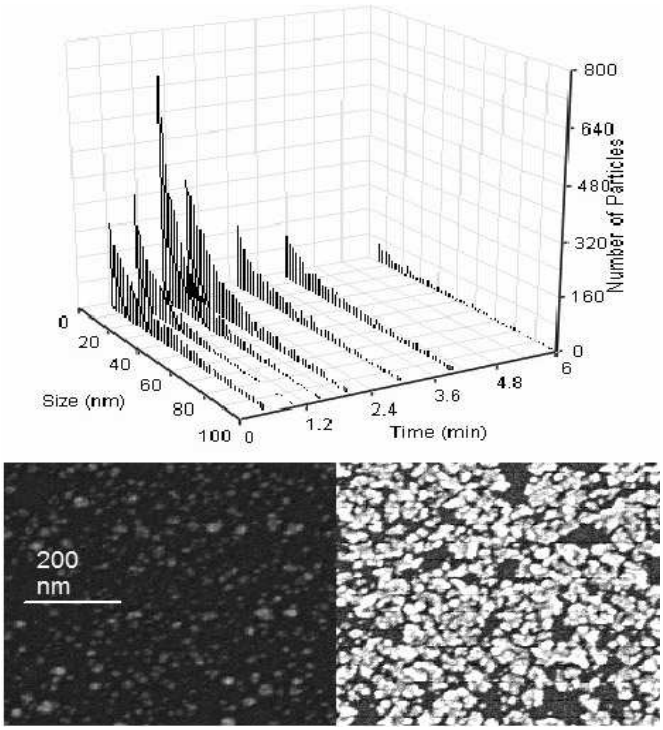

Fig. 10. The upper panel: the variation of the particle size distribution as a function of the X-ray dose (exposure time). The lower panel: the SEM images taken on a 0.5-min exposure deposition (left) and a 6-min exposure deposition (right) [10].

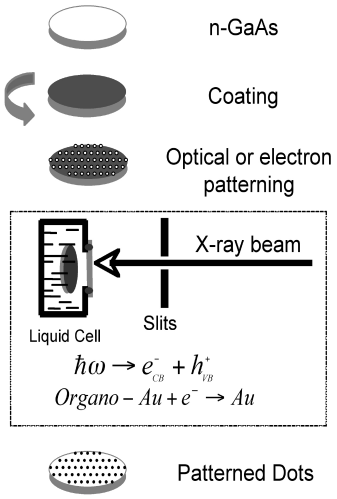

Fig. 11. The patterning process on n-GaAs using the X-ray induced metal deposition method [10].

Figure 12 shows a series of experimental results.

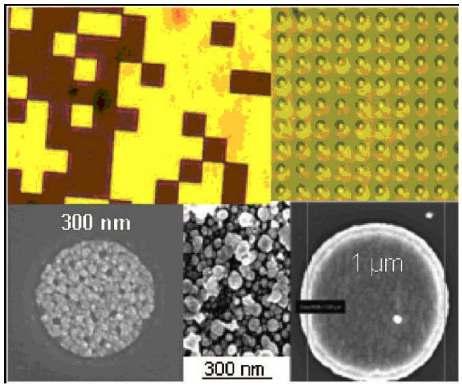

Fig. 12. The Au pattern deposition on n-GaAs with feature dimensions ranging from microns to submicron. The upper left: the deposition showing the positive and negative patterns. The upper right: the 1-μm Au dot array deposition and the lower right: the details of a 1-μm Au dot. The lower center: the detailed image of Au deposition using the optical mask. The lower left: a 300-nm dot deposition prior to the removal of the PMMA [10].

On the upper left (Fig. 12), the optical micrograph of a pattern deposition is shown, that was obtained with 23-min X-ray exposure. The Au deposition thickness is 66 nm, which gives a deposition rate of about 3 nm/min. The smallest feature dimension on the pattern is 1 μm, and the features are faithful to the mask quality. On the upper right, a pattern deposition made of the arrays of 1-μm gold dots is shown. It was obtained with 10-min X-ray exposure, and the dot height is about 32 nm. On the bottom right and center, the details of a 1-μm dot are shown with the SEM images.

AFM measurements indicate that the wall roughness is within the sizes of the particles and the wall steepness is about 60°. The bottom left image shows the deposition in a smaller feature (300 nm) prior to removal of the PMMA. Growth in more confined areas, i.e., smaller dimension features down to a few nanometers will be vigorously pursued in the future studies.

The particle sizes in these depositions range from a few nanometers at the smaller end to ∼30 nanometers at the larger end. The future studies will also focus on the control of the particle sizes, using, *e.g.*, more diluted solution and/or addicts as stabilizer.

The process is photoelectrochemical in nature, and may be applied readily to other semiconductor systems [10, 15].

4. Conclusions

In summary, a synchrotron X-ray induced, substrate-carrier-mediated metal deposition process on SiO_2 and GaAs surfaces is described.

The energy of the beam and the solution conditions permit the control of the Au nanoparticle deposition. The height of the nanoparticles remains nearly constant, and the diameter of the nanoparticles increases with increasing dose. The distribution is more uniform at higher energy and higher dilution, and agglomerated deposition of particles appears at high dose.

Addition of surfactants (nonionic: Triton X-100, anionic: SDS sodium dodecyl sulfate) at Neutronex solution has not suppressed nanoparticle cluster appearance. A narrow size distribution in the sub-5 nm size range has been obtained with a capping agent (alkyl thioether end-functionalized poly(methacrylic acid) in 0.5 mM hydrogen tetrachloroaurate solution.

Patterned deposition of metallic nanoclusters can be obtained on a silicon dioxide surface using an X-ray mask. In this case the deposited structure resolution depends upon the X-ray masking performance. The GaAs n-type samples were used to achieve direct nanopatterned deposition of metallic nanoparticles by a combined use of bottom-up X-ray induced self-assembly of nanoparticles, and by top-down electron beam lithography. The metal nanoparticles are deposited in the non-X-ray-exposed area, thus self-assembling in the polymer pattern. In this case the deposited structure resolution depends upon the e-beam lithography performance.

Future studies will focus on metal deposition in more confined areas and on the particle size control. A *dual* process on GaAs that involves both etching and deposition to make structural devices will also be attempted.

Acknowledgements. The authors would like to thank Lahsen Assoufid for AFM measurements. Part of this work was performed at the DuPont-Northwestern-Dow Collaborative Access Team (DND-CAT) Synchrotron Research Center located at Sector 5 of the Advanced Photon Source. Part of this work was carried out at the Center for Nanoscale Materials, Argonne National Laboratory. DND-CAT is supported by the E.I. DuPont de Nemours & Co., The Dow Chemical Company, the U.S. National Science Foundation through Grant DMR-9304725 and the State of Illinois through the Department of Commerce and the Board of Higher Education Grant IBHE HECA NWU 96.

References

[1] ZHANG Y., ASAHINA S., YOSHIHARA S., SHIRAKASHI T., *Oxygen reduction on Au nanoparticle deposited boron-doped diamond films*, Electrochimica Acta **48**, pp. 741–747, 2003.

[2] MATTHEY D., WANG J.G., WENDT S., MATTHIESEN J., SCHAUB R., LAEGSGAARD E., HAMMER B., BESENBACHER F., *Enhanced Bonding of Gold Nanoparticles on Oxidized* $TiO_2(110)$, Science **315**, pp. 1692–1696, 2007.

[3] SELVARAJ V. ALAGAR, M., HAMERTON I., *Analytical detection and biological assay of antileukemic drug using gold nanoparticles*, Electrochimica Acta **52**, pp. 1152–1160, 2006.

[4] TIRELLI N., *(Bio)Responsive nanoparticles*, Current Opinion in Colloid & Interface Science, **11**(4), pp. 210–216, 2006.

[5] PACIOTTI G.F., KINSTON D.G.I., TAMARKIN L., *Colloidal gold nanoparticles: A novel nanoparticle platform for developing multifunctional tumor-targeted drug delivery vectors*, Drug Develop. Res. **67** (1), pp. 47–54, 2006.

[6] YANG Y.C., WANG C.H., HWU Y.K., JE J.H., *Synchrotron X-ray synthesis of colloidal gold particles for drug delivery*, Materials Chemistry and Physics **100** (1), pp. 72–76, 2006.

[7] ROSENBERG R.A., MA Q., LAI B., MANCINI D.C., *Surface photochemistry induced by X-ray irradiation*, J. Vac. Sci. Technol. B **16**, no. 6, pp. 3535–3538, 1998.

[8] MA Q., MOLDOVAN N., MANCINI D.C., ROSENBERG R.A.,*Synchrotron-radiation-induced, selective-area deposition of gold on polyimde from solution*, Appl. Phys. Lett. **76**, no. 15, pp. 2014–2016, 2000.

[9] DIVAN R., MANCINI D.C., MOLDOVAN N., ASSOUFID L., CHU Y.S., MA Q., ROSENBERG R.A., *X-ray Patterned Deposition of Gold Nanoparticles from Solution*, *International Conference for Semiconductors (IEEE co-sponsored)*, CAS 2003, Sinaia, Romania, pp. 39–42, 2003.

[10] MA Q., DIVAN R., MANCINI D.C., KEATON D.T., ROSENBERG R.A., QUITANA J.P., *X-ray induced substrate-carrier mediated deposition of metal on GaAs*, Appl. Phys. Lett. **89**, 2006, 083114.

[11] MULVANEY P., *Surface Plasmon Spectroscopy of Nanosized Metal Particles*, Langmuir **12**, pp. 788–800, 1996.

[12] DIVAN R., MANCINI D.C., GALLAGHER S.M., BOOSKE J., VAN DER WEIDE D., *Improvements in Graphite-Based X-ray Mask Fabrication for Ultra-Deep X-ray Lithography*, Microsystem Technologies, **10**(10), pp. 728–734, 2004.

[13] HUSSAIN I., GRAHAM S., WANG Z., TAN B., D.C. SHERRINGTON, S.P. RANNARD, A.I. COOPER, M. BRUST, *Size-Controlled Synthesis of Near-Monodisperse Gold Nanoparticles in the 1-4 nm Range Using Polymeric Stabilizers*, J.Am.Chem.Soc, **127**, pp. 16398-16399, 2005.

[14] VALIENTE M., RODENAS E., *Influence of cetyltrimethylammonium bromide/1-hexanol and cetyltrimethylammonium bromide/1-octanol mixed micelles on the basic hydrolysis of crystal violet*, Langmuir, **6**, pp. 775–782, 1990.

[15] MA Q., MANCINI D.C., ROSENBERG R.A., *Synchrotron-radiation-induced anisotropic wet etching of GaAs*, Appl. Phys. Lett. **75**, pp. 2274–2276, 1999.

[16] LIZ-MÁRZAN L.M., LADO-TOURINO I., *Reduction and Stabilization of Silver Nanoparticles in Ethanol by Nonionic Surfactants*, Langmuir, **12**, pp. 3585–3589, 1996.

[17] CHIANG C.L., *Controlled Growth of Gold Nanoparticles in AOT/*$C_{12}E_4$*/Isooctane Mixed Reverse Micelles*, Journal of Colloid and Interface Science, **239**, pp. 334–341, 2001.

[18] KAWASAKI H., NISHIMURA K., ARAKAWA R., *Influence of the Counterions of Cetyltrimetylammonium Salts on the Surfactant Adsorption onto Gold Surfaces and the Formation of Gold Nanoparticles*, J.Phys.Chem.C, **111**, pp. 2683–2690, 2007.

[19] AUER S., FRENKEL D., *Prediction of absolute crystal-nucleation rate in hard-sphere colloids*, Nature **409**, pp. 1020–1023, 2001.

[20] MA Q., MOLDOVAN N., MANCINI D.C., ROSENBERG R.A., *Wet etching of GaAs using synchrotron radiation X rays*, J. of Appl. Phys. **89**(5), pp. 3033–3040, 2001.

[21] VAN DE VEN J., NABBEN H.J., *Anisotropic Photoetching of III–V Semiconductors, J. Electrochem. Soc.* **137**(5), pp. 1603–1610, 1990.

[22] ROBERTO M.N., ZHANG X., SCARMOZZINO R., WILLNER A.E., PODLESNIK D.V., OSGOOD JR. R.M., *The Laser-Controlled Micrometer-Scale Photoelectrochemical Etching of III–V Semiconductors*, J. Electrochem. Soc. **138** (4), pp. 1174–1185, 1991.

[23] HOISTY R.W., *Photoetching and Plating of Gallium Arsenide*, J. Electrochem. Soc. **108**(8), pp. 790–794, 1961.